Journal of Alloys and Compounds 512 (2012) 144–148

Contents lists available at SciVerse ScienceDirect

Journal of Alloys and Compounds

journal homepage: www.elsevier.com/locate/jallcom

A new yellowish-green-emitting phosphor: Eu^{2+}-doped $K_4CaSi_3O_9$

Beiling Yuan [a], Xigang Wang [a], Taiju Tsuboi [b], Yanlin Huang [a,*], Hyo Jin Seo [c,*]

[a] College of Chemistry, Chemical Engineering and Materials Science, Soochow University, Suzhou 215123, China
[b] Faculty of Engineering, Kyoto Sangyo University, Kamigamo, Kyoto 603-8555, Japan
[c] Department of Physics, Pukyong National University, Busan 608-737, Republic of Korea

ARTICLE INFO

Article history:
Received 12 May 2011
Received in revised form
17 September 2011
Accepted 19 September 2011
Available online 4 October 2011

Keywords:
Luminescence
Eu^{2+}
Optical materials and properties
Silicate

ABSTRACT

Eu^{2+}-activated $K_4CaSi_3O_9$ phosphors were synthesized by conventional solid-state reaction. The phase formation was confirmed by X-ray powder diffraction measurements. The photoluminescence excitation and emission spectra were investigated. The phosphor presents bright yellowish-green-emitting luminescence under the excitation of UV and near UV light. The luminescence absolute quantum efficiencies of the phosphors with different Eu^{2+}-doping levels (1.0–5.0 mol%) were measured. The crystal structure and the site-occupancy of Eu^{2+} ions doped in $K_4CaSi_3O_9$ crystal lattice were discussed. Two different Eu^{2+} centers were assigned according to the crystal structure and the luminescence characteristics. The dependence of luminescence intensity on temperatures (25–150 °C) was measured. The chromaticity coordinates and activation energy (ΔE) for thermal quenching were reported. The phosphor shows an excellent thermal stability on temperature quenching.

1. Introduction

The absorption and emission spectra of Eu^{2+} usually comprise broad bands due to transitions between the $4f^7$ ground state and the crystal field components of the $4f^65d^1$ excited state configuration. The emission bands of Eu^{2+} strongly depend on the host crystal and vary from ultraviolet to red. It has been reported that the long-wavelength emission of Eu^{2+} in some alkaline earth silicates with a chain arrangement of alkaline earth ions is due to the preferential orientation of one d orbital of Eu^{2+} [1].

The luminescence properties of Eu-doped solids have been intensively investigated during the past decade [2–7]. In recent years, Eu^{2+}-doped phosphors have been paid great attentions due to the significant applications as phosphors in white light-emitting diodes (W-LEDs), for example, the nitrides and oxynitrides-based compounds have been demonstrated to be excellent for W-LEDs application [8–11]. However, the very high firing temperatures and high nitrogen pressures are required for their synthesis, resulting in higher production cost.

Eu^{2+}-doped silicate phosphors can absorb ultraviolet or blue (380–460 nm) light from LEDs chips and emit visible light. Many studies on Eu^{2+}-activated silicates have been published [12–14], e.g., $SrSiO_3:Eu^{2+}$ [15], $Sr_2SiO_4:Eu^{2+}$ [16], $M_3SiO_5:Eu^{2+}$ (M = Sr, Ba) [17], $MSi_2O_5:Eu^{2+}$ (M = Ca, Sr, Ba) [18], $SrCaSiO_4:Eu^{2+}$ [19], $BaZn_2Si_2O_7:Eu^{2+}$ [20], $BaCa_2MgSi_2O_8:Eu^{2+}$ [21], $M_3MgSi_2O_8:Eu^{2+}$ (M = Ca, Sr, Ba) [22], $Li_2SrSiO_4:Eu^{2+}$ [23], $Ca_3SiO_4Cl_2:Eu^{2+}$ [24], $CaAl_2Si_2O_8:Eu^{2+}$ [25], $M_2MgSi_2O_7:Eu^{2+}$ (M = Ca, Sr, Ba) [26], etc.

Gunawardane and Glasser [27] first reported the basic crystallographic data of unit cell parameters of $K_4CaSi_3O_9$. Recently, Arroyabe et al. [28] have investigated the detailed crystal structure of $K_4CaSi_3O_9$ by X-ray diffraction techniques and Raman spectroscopy. According to the connectivity of the $[SiO_4]$-tetrahedra, $K_4CaSi_3O_9$ is assigned to the group of cyclosilicates with space group $pa\bar{3}$, which is isostructural with form *I* of $K_4SrSi_3O_9$ with $[Si_{12}O_{36}]$-rings centered on the $\bar{3}$ axes. Fig. 1 is the schematic view of the $K_4CaSi_3O_9$ structure along *c*-direction, which was modeled using the Diamond Crystal and Molecular Structure Visualization software on the basis of the atomic coordinate data reported by Arroyabe et al. [28]. The distorted octahedra of CaO_6 form the chain arrangements in the tunnels parallel to *c* axis (Fig. 1).

In this work $K_4CaSi_3O_9:Eu^{2+}$ phosphors were synthesized by the conventional solid state reaction. The structure was investigated by powder X-ray powder diffraction (XRD) measurements. The photoluminescence excitation and emission spectra, and the decay curves were measured. The luminescence intensity measurements were performed as a function of temperature. The activation energy for thermal quenching (ΔE) was calculated. The crystal structure of $K_4CaSi_3O_9$ and the site-occupations of Eu^{2+} ions in the crystal lattice were discussed.

2. Experimental details

The preparation of $K_4CaSi_3O_9:Eu^{2+}$ was carried out by solid state synthesis. The raw materials were high-purity K_2CO_3, $CaCO_3$, SiO_2 and Eu_2O_3. The doping level

* Corresponding authors.
E-mail addresses: huang@suda.edu.cn, huangyanlin@hotmail.com (Y. Huang), hjseo@pknu.ac.kr (H.J. Seo).

0925-8388/$ – see front matter © 2011 Elsevier B.V. All rights reserved.
doi:10.1016/j.jallcom.2011.09.050

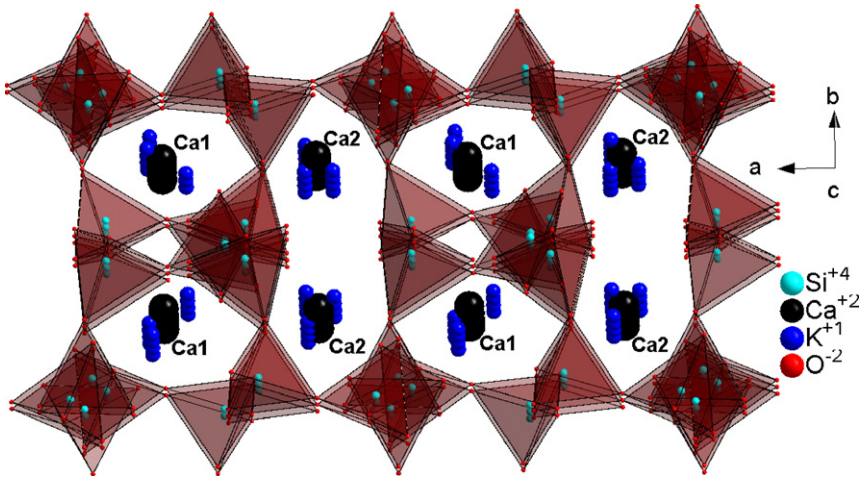

Fig. 1. The schematic views of the $K_4CaSi_3O_9$ structure along *c*-direction.

of Eu^{3+} is 1.0–5.0 mol%. The starting materials with stoichiometric amounts were ground together in an agate mortar. The mixture was first heated up to 800 °C and kept at this temperature for 6 h. After a second homogenization in the mortar, the sample was heated up to 850 °C and kept at this temperature for 10 h. After that, the sample was mixed and heated at 950 °C for 10 h in crucibles along with the reducing agent (active carbon).

The XRD pattern was collected on a Rigaku D/Max-2000 diffractometer operating at 40 kV, 30 mA with Bragg–Brentano geometry by using Cu Kα radiation (λ = 1.5418 Å). The optical excitation and emission spectra were recorded by a Perkin-Elmer LS-50B luminescence spectrometer and a Hitachi F-4500 fluorescence spectrophotometer. The luminescence decay curves was measured using the third harmonic (355 nm) of a pulsed Nd:YAG laser. To study thermal quenching of the luminescence, the same spectrofluorimeter was equipped with a homemade heating cell. The luminescence quantum efficiency (QE) was measured by an Absolute Photoluminescence Quantum Yield Measurement System (C9920-02, Hamamatsu) with an integrating sphere, which allows obtaining the absolute QE value. The excitation was done by changing excitation wavelength of light from 150 W Xe-lamp.

3. Results

3.1. The crystal phase formation

The samples were checked by powder XRD measurements (Fig. 2). X-ray powder diffraction patterns of the pure and Eu^{2+}-doped $K_4CaSi_3O_9$ well match the PDF2 card number 39-1427 ($K_4CaSi_3O_9$) in the International Center for Diffraction Data (ICDD) database. No impurity lines were observed, and all the reflections could be well indexed to a $K_4CaSi_3O_9$ single phase.

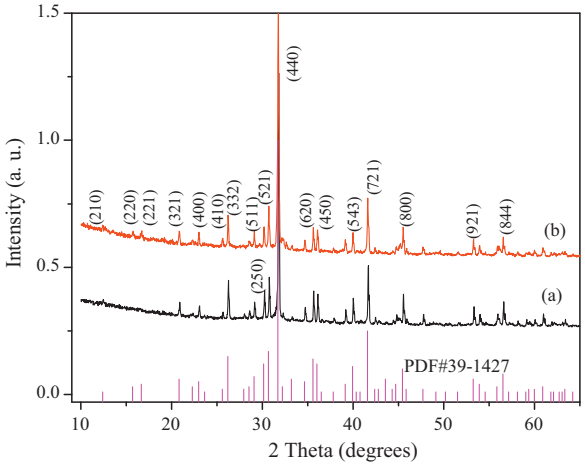

Fig. 2. XRD patterns of pure (a) and Eu^{2+}-doped $K_4CaSi_3O_9$ compared with JCPDs card No.39-1427.

3.2. Photoluminescence spectra and the Eu^{2+} centers

Fig. 3(a) presents the excitation and emission spectra of $K_4CaSi_3O_9$:Eu^{2+} at room temperature. The emission spectrum has a broad emission band (450–700 nm) with a maximum at about 530 nm, which can be ascribed to $4f^65d \rightarrow 4f^7$ ($^8S_{7/2}$) transition of Eu^{2+} ions. The excitation spectra consist of the broad absorption bands from 250 to 450 nm attributed to 4f–5d transition of Eu^{2+} ions (Fig. 3(a)). This indicates that the phosphor can well match with the light of UV-LED chips (360–400 nm), which is essential for improving the efficiency of W-LEDs. The CIE (Commission Internationale de l'Eclairage) coordinates were calculated from the emission spectra to be ($x = 0.319$, $y = 0.573$), which is a typical yellowish-green emission.

The asymmetric emission spectra (ex = 355 nm) in Fig. 3(a) imply that Eu^{2+} ions occupy more than one site in the lattice, which can be deconvoluted into at least two Gaussian components peaked at 530 nm (referred to as Eu2) and 586 nm (referred to as Eu1). This indicates that there are two Eu^{2+} luminescence centers in $K_4CaSi_3O_9$ lattices. The different excitation spectra (Fig. 4) and luminescence decay (lifetimes) (Fig. 5) for the two emission bands (530 and 586 nm) testify two distinct Eu^{2+} centers in $K_4CaSi_3O_9$ lattices.

Fig. 3(b) exhibits the crystallographic structure of Ca^{2+} sites in $K_4CaSi_3O_9$. Ca1 shares three O(4) and three O(5), while Ca2 shares three O(1) and three O(2). Each kind of Ca^{2+} sites has different average distance between the cation and ligands: Ca(1)–O(4) 2.429 Å × 3 and Ca(1)–O(5) 2.393 Å × 3; Ca(2)–O(1) 2.429 Å × 3 and Ca(2)–O(2) 2.444 Å × 3. In $K_4CaSi_3O_9$, Ca1 surrounded by six nearest oxygen neighbors in form of octahedral, which is more heavily distorted than that of Ca2 site. Usually, the crystal field strength, presented as D_q, is inversely proportional to the 5th power of the bond-length *R* [29].

$$D_q \propto 1/R^5 \quad (1)$$

When the crystal environments are analogous, a shorter bond distance implies stronger crystal field strength. Accordingly, the decrease of the barycenter of excitation band is much higher with nephelauxetic effect and crystal field on the $4f^65d^1 \rightarrow 4f^7$ transition of Eu^{2+} [26]. Thus, the high-energy emission 530 nm (Eu2) originates from the Eu^{2+} ions which occupy loose crystal circumstance with larger Ca–O bond length (Ca2 site); and the low-energy emission 586 nm (Ca1 site) are ascribed to the Eu^{2+} ions occupying compact crystal circumstance with shorter Ca–O bond length (Ca1).

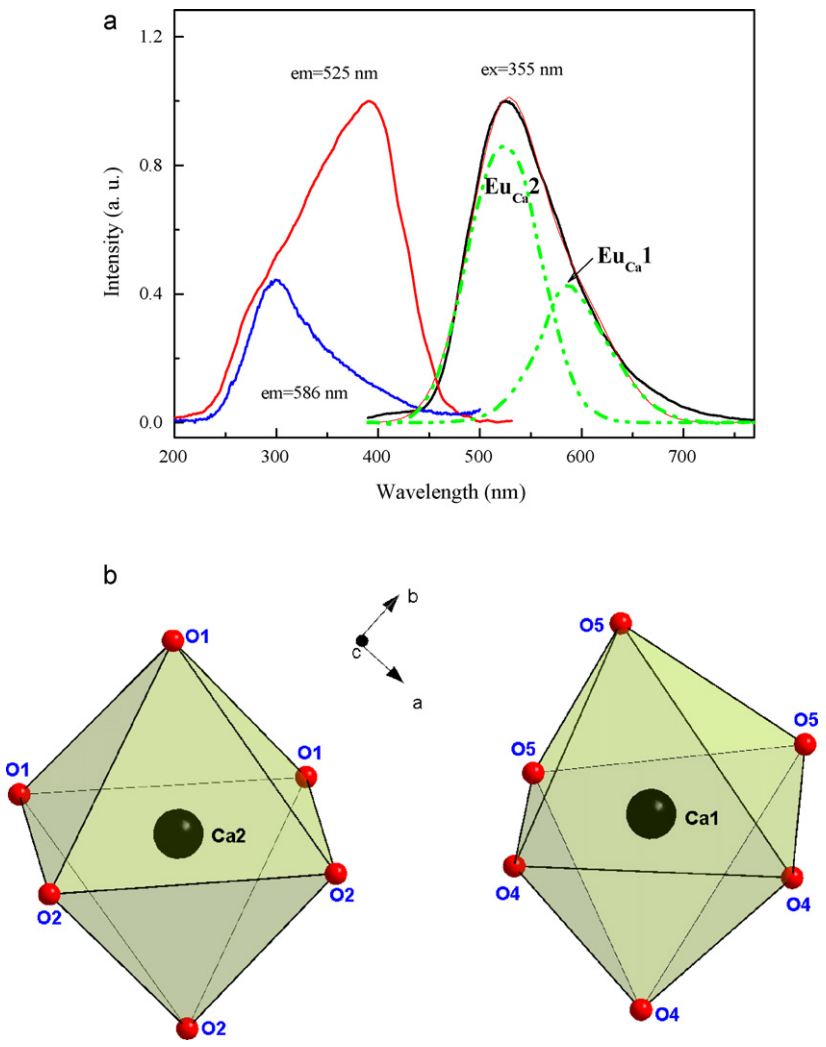

Fig. 3. (a) The emission spectra of the $K_4CaSi_3O_9:Eu^{2+}$ (λ_{ex} = 355 nm) and the excitation spectra by monitoring the emission wavelength at λ_{em} = 530 nm and 586 nm. (b) The comparison of the coordination geometries around the Ca1 and Ca2.

Although the environment of Eu1 is not so big different from that of Eu2, the distortion of octahedral gives an intense influence on the excited energy states of Eu^{2+}, which leads to the emission energy difference of about 0.22 eV (i.e., the 586 nm (2.116 eV) Eu1 emission of Eu1 with largely distorted octahedral for the 530 nm (2.339 eV) emission of Eu2 with less-distorted octahedral).

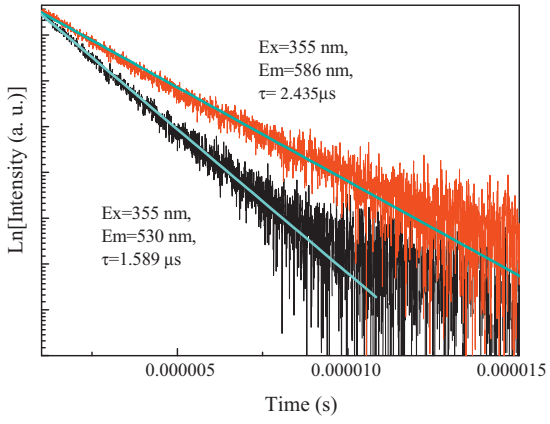

Fig. 4. The decay curves of emission bands at 530 nm and 586 nm under the excitation of 355 nm.

When $K_4CaSi_3O_9:Eu^{2+}$ is laid up in air atmosphere, it presents a little bit sensitivity to moisture. Certainly this is a drawback for its application. It has been reported that surface coatings with silica nano-particles on Eu^{2+}-doped silicate phosphors [30] or the addition of a flux [31] can improve its stability of moisture-resistance. New experiments will be conducted to enhance its stability with respect to water.

The photoluminescence QEs of $K_4CaSi_3O_9:Eu^{2+}$ with doping concentrations of 1.0, 3.0, 4.0, and 5.0 mol% were measured and listed in Table 1. By taking into account the results of excitation spectra in Fig. 3(a), the excitation wavelength for QEs measurements was selected at 320 nm because of the good overlapping between the excitation spectra of the 586 nm (Eu1 emission) and the 530 nm bands (Eu2 emission). The QE of $K_4CaSi_3O_9:Eu^{2+}$ 3.0 mol% was measured to be 39.9% at the excitation of 320 nm light

Table 1
The quantum efficiencies at *RT* of $K_4CaSi_3O_9:Eu^{2+}$.

Doping level (mol%)	Excitation (nm)	QE (%)	Measured range (nm)
1.0	320	33.7	385–800
3.0	320	39.9	400–800
4.0	320	14.5	400–800
5.0	320	11.8	400–800

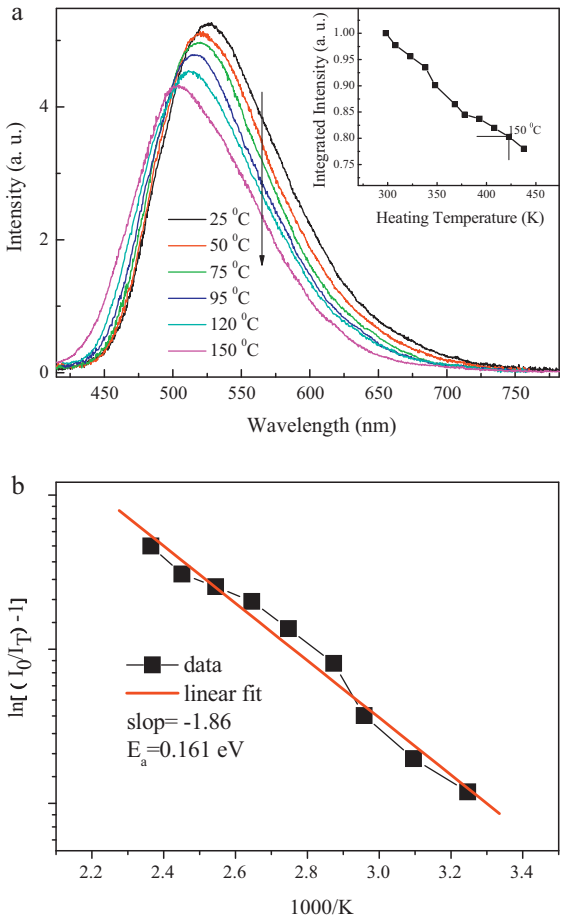

Fig. 5. (a) The emission spectra of $K_4CaSi_3O_9:Eu^{2+}$ at the selected temperatures from 25 to 150 °C under excitation of 365 nm; the insert is the integrated emission intensity normalized with respect to the value at 25 °C; (b) the activation energies of the thermal quenching fitted in Eq. (2).

at 300 K. The luminescence presents quenching as increasing the doping level of Eu^{2+}. It is noted that the QE value of $K_4CaSi_3O_9:Eu^{2+}$ is not so high and lower than the reported commercial phosphors. However, this could be further enhanced by improving the synthesis conditions to reduce the number of defects and impurities.

3.3. Dependence of luminescence on temperature

The temperature-dependent luminescence spectra of $K_4CaSi_3O_9:Eu^{2+}$ under the excitation of 365 nm are shown in Fig. 5(a). The intense broad peak is originated from 5d–4f transition of Eu^{2+} ions. With increase in temperature the thermal quenching is observed. The temperature dependent emission intensities normalized to the intensity at 25 °C are shown in inset in Fig. 5(a). The emission intensity is decreased to 80% of the initial value at 25 °C. It has been reported that with increasing temperature at 150 °C YAG:Ce^{3+} (yellow phosphor 560 nm) is 94%, $(Sr_{1.7}Ba_{0.2}Eu_{0.1})SiO_4$ (yellow phosphor 575 nm) is 49%, $(Ba_{1.1}Sr_{0.7}Eu_{0.2})SiO_4$ (green phosphor 528 nm) is 77% and $(Sr_{0.82}Ba_{0.15}Eu_{0.03})_2Si_5N_8$ (red phosphor 632 nm) is 87% of its 25 °C values, respectively [29]. The results in this experiment show that $K_4CaSi_3O_9:Eu^{2+}$ has a good thermal stability on temperature quenching effect.

The thermal activation energy (ΔE) for the thermal quenching of the Eu^{2+} emission was determined by measuring the temperature dependence of the Eu^{2+} emission intensity. The temperature

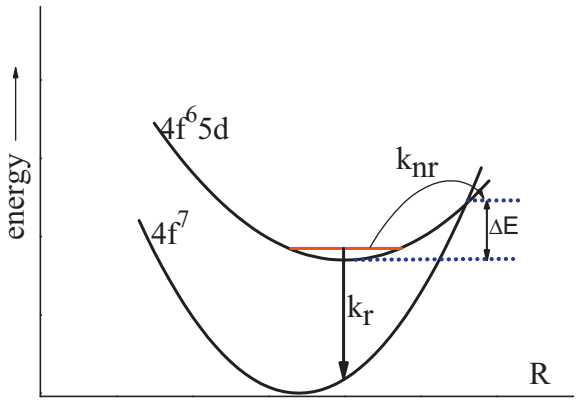

Fig. 6. The schematic configuration coordinate diagram for the excited state level $4f^65d$ and the ground state $4f^7$ of Eu^{2+} ion.

dependence of the luminescence intensity is described by a modified Arrhenius equation as follows [7]:

$$I_T = \frac{I_0}{1 + c\exp(-\frac{\Delta E}{kT})} \quad (2)$$

where I_0 is the initial emission intensity, I_T is the intensity at different temperatures, ΔE is the activation energy of thermal quenching, c is a constant for a certain host, and k is the Boltzmann constant (8.629×10^5 eV). The activation energy is the energy required to raise the electron from the relaxed excited level into the host lattice conduction band.

Fig. 5(b) plots of $\ln[(I_0/I_T) - 1]$ vs. $1000/T$, which is linear with a slope of −1.86. According to Eq. (2), the activation energy ΔE was calculated to be 0.161 eV. This mechanism can be illustrated by Fig. 6, in which the schematic configuration coordinate diagram for the excited state level $4f^65d$ and the ground state $4f^7$ of Eu^{2+} ion is presented. ΔE is the activation energy, and R means the Eu^{2+}-ligand distance. This illustrates the radiative transition k_r and non-radiative (i.e., thermal phonon-assisted) transition k_{nr} from the excited state.

Fig. 7 displays the temperature dependence of the full wavelength at half maximum (FWHMs) and emission positions of Eu^{2+} in $K_4CaSi_3O_9$. It can be observed that as the temperature is increased the emission band (FWHM) is broadened, and the emission peaks show blue-shift from 530 to 505 nm. This is not advantageous because this could change the color chromaticity.

The blue-shifted emission spectra of Eu^{2+} with increasing temperature have been well described in the host where Eu^{2+} ions

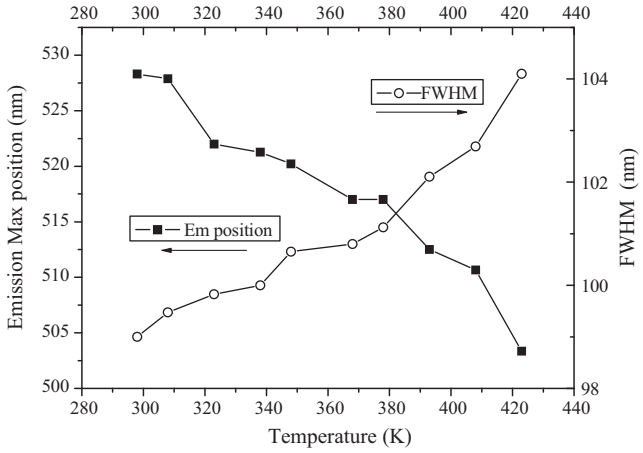

Fig. 7. The temperature dependence of the central emission positions and FWHMs in the emission of $K_4CaSi_3O_9:Eu^{2+}$ in Fig. 5(a).

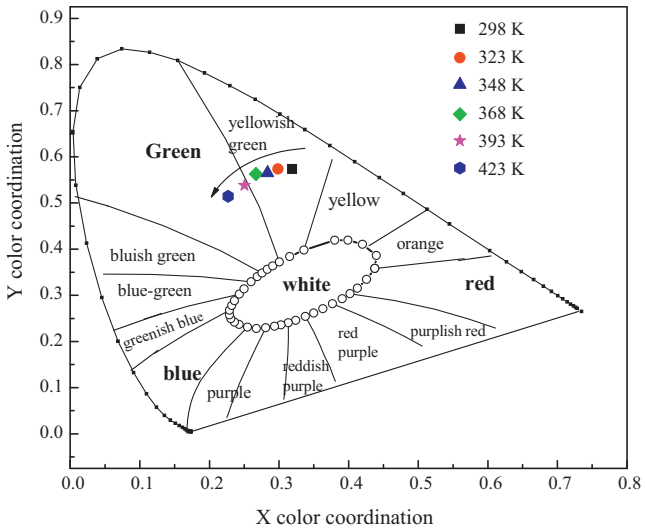

Fig. 8. CIE chromaticity coordinates of $K_4CaSi_3O_9:Eu^{2+}$ at various temperatures in Fig. 5(a).

occupy two kinds of luminescence centers, e.g., $(Sr, Ca)_2SiO_4:Eu^{2+}$ [32], $(Sr_{0.82}Ba_{0.15}Eu_{0.03})_2Si_5N_8$ and $(Sr_{1.7}Ba_{0.2}Eu_{0.1})SiO_4$ [29], etc. The thermal phonon-assisted tunneling model has been applied to elucidate this phenomenon. The thermally active phonon-assisted tunneling from the excited states of low-energy (Ca1) emission band to the excited states of high-energy (Ca2) emission band in the configuration coordinate diagram increases with an increase of temperature. The energy transfers from the Ca1 site to Ca2 site through the phonon-assisted tunneling by overcoming an energy barrier and finally reverts to the ground state to give a shorter wavelength emission.

The CIE coordinates were calculated from emission spectra at different temperature in Fig. 8. With increasing of temperature, the CIE coordinates slightly shift from (0.319, 0.573) to (0.226, 0.514), which is consistent with the blue-shift of emission spectra. This is a shortcoming of $K_4CaSi_3O_9:Eu^{2+}$ for the possible application as a LEDs phosphor at higher temperature.

4. Conclusions

The phosphors of Eu^{2+}-doped $K_4CaSi_3O_9$ were synthesized by high temperature solid state reaction method. The photoluminescence excitation spectrum shows a very broad band extending from 250 to 450 nm. $K_4CaSi_3O_9:Eu^{2+}$ presents yellowish-green color with CIE coordinates of ($x = 0.319$, $y = 0.573$) under the excitation of near UV light. There are two kinds of Eu^{2+} luminescence centers at 530 nm (Eu2) and 586 nm (Eu1), which occupy Ca2 and Ca1 sites, respectively, in $K_4CaSi_3O_9$ lattices. The results of temperature dependent luminescence spectra show that $K_4CaSi_3O_9:Eu^{2+}$ has an excellent thermal stability on the temperature quenching. The activation energy ΔE was calculated to be 0.161 eV. With increasing of temperature, the emission bands show the blue-shift with increasing bandwidth. This blue-shift was described in terms of the thermal phonon-assisted tunneling model.

Acknowledgments

This work was supported by the Mid-career Researcher Program through National Research Foundation of Korea (NRF) grant funded by the Ministry of Education, Science and Technology (MEST) (Project No. 2009-0078682) and by A Project Funded by the Priority Academic Program Development of Jiangsu Higher Education Institutions (PAPD). One of the authors (Yanlin Huang) thanks Mr. Yosuke Nakai in Kyoto Sangyo University for helping the measurements of PL quantum efficiencies.

References

[1] P. Dorenbos, J. Lumin. 104 (2003) 239–260.
[2] X. He, M. Guan, C. Zhang, T. Shang, N. Lian, Y. Yao, J. Alloys Compd. 509 (2011) L341–L343.
[3] Y. Tan, Z. Fang, W. Chen, P. He, J. Alloys Compd. 509 (2011) 6321–6324.
[4] V.Y. Yulia, A.V. Tolmachev, M.V. Dobrotvorskaya, O.M. Vovk, J. Alloys Compd. 509 (2011) 5320–5325.
[5] H. Wu, Y. Hu, L. Chen, X. Wang, J. Alloys Compd. 509 (2011) 4304–4307.
[6] J. Mrázek, L. Spanhel, M. Surýnek, M. Potel, V. Matějec, J. Alloys Compd. 509 (2011) 4018–4024.
[7] R.J. Xie, N. Hirosaki, N. Kiumra, K. Sakuma, M. Mitomo, Appl. Phys. Lett. 90 (2007) 191101–191103.
[8] B. Lei, K. Machida, T. Horikawa, H. Hanzawa, Chem. Lett. 39 (2) (2010) 104–105.
[9] B. Lei, K. Machida, T. Horikawa, H. Hanzawa, Chem. Lett. 40 (2) (2011) 140–141.
[10] V.D. Luong, W. Zhang, H.R. Lee, J. Alloys Compd. 509 (7) (2011) 7525–7528.
[11] K. Shioi, Y. Michiue, N. Hirosaki, R.J. Xie, T. Takeda, Y. Matsushita, M. Tanaka, Y. Qiang Li, J. Alloys Compd. 509 (12) (2011) 332–337.
[12] H.L. Li, R.J. Xie, N. Hirosaki, T. Takeda, Int. J. Appl. Ceram. Technol. 6 (4) (2009) 459–464.
[13] I. Baginskiya, R.S. Liu, J. Electrochem. Soc. 156 (2009) G29–G32.
[14] Y.S. Tang, S.F. Hu, C.C. Lin, N.C. Bagkar, R.S. Liu, Appl. Phys. Lett. 93 (2008) 131114–131116.
[15] Z. Cui, R. Ye, D. Deng, Y. Hua, S. Zhao, G. Jia, C. Li, S. Xu, J. Alloys Compd. 509 (8) (2011) 3553–3558.
[16] Y. Gu, Q. Zhang, Y. Li, H. Wang, J. Alloys Compd. 509 (6) (2011) L109–L112.
[17] J.K. Park, K.J. Choi, J.H. Yeon, S.J. Lee, C.H. Kim, Appl. Phys. Lett. 88 (4) (2006) 043511–043513.
[18] K.I. Seo, J.H. Park, J.S. Kim, Y.H. Na, J.C. Choi, J.S. Bae, Solid State Commun. 149 (2009) 1578–1581.
[19] H. Yu, Y. Lai, G. Gao, L. Kong, G. Li, S. Gan, G. Hong, J. Alloys Compd. 509 (23) (2011) 6635–6639.
[20] S. Yao, L. Xue, Y. Yan, J. Alloys Compd. 509 (5) (2011) 1870–1873.
[21] Y. Yonesaki, Q. Dong, N.S.B. Mohamad, A. Miura, T. Takei, J. Yamanaka, N. Kumada, No. Kinomura, J. Alloys Compd. 509 (35) (2011) 8738–8741.
[22] J.S. Kim, Y.H. Park, J.C. Choi, H.L. Park, Electrochem. Solid State Lett. 8 (2005) H65–H67.
[23] T.G. Kim, H.S. Lee, C.C. Lin, T. Kim, R.S. Liu, T.S. Chan, S.J. Im, Appl. Phys. Lett. 96 (2010) 061904–061906.
[24] J. Liu, H.Z. Lian, J.Y. Sun, C.S. Shi, Chem. Lett. 34 (2005) 1340–1341.
[25] W.J. Yang, L.Y. Luo, T.M. Chen, N. Wang, Chem. Mater. 17 (2005) 3883–3888.
[26] S.H.M. Poort, H.M. Reijnhoudt, H.O.T. van der Kuip, G. Blasse, J. Alloys Compd. 241 (1996) 75–81.
[27] R.P. Gunawardane, F.P. Glasser, Z. Anorg. Allg. Chem. 411 (1975) 163–171.
[28] E. Arroyabe, R. Kaindl, V. Kahlenberg, Z. Anorg. Allg. Chem. 635 (2009) 337–345.
[29] L. Chen, C.C. Lin, C.W. Yeh, R.S. Liu, Materials 3 (2010) 2172–2195.
[30] J. Zhuang, Z. Xia, H. Liu, Z. Zhang, L. Liao, Appl. Surf. Sci. 257 (2011) 4350–4353.
[31] C.C. Lin, R.S. Liu, J. Phys. Chem. Lett. 2 (2011) 1268–1277.
[32] J.S. Kim, Y.H. Park, S.M. Kim, J.C. Choi, H.L. Park, Solid State Commun. 133 (2005) 445–448.